

CO₂ CORROSION INHIBITOR PERFORMANCE IN THE PRESENCE OF SOLIDS: TEST METHOD DEVELOPMENT

Anette Pedersen,¹ Katerina Bilkova,² Egil Gulbrandsen³, Jon Kvarekvål
Institute for Energy Technology (IFE)
P.O. Box 40
NO-2027, Kjeller, Norway

ABSTRACT

The background and development of three test methods for CO₂ corrosion inhibitors in presence of solids are described: 1) Inhibitor performance testing in the presence of suspended solids; 2) Inhibitor performance testing on steel covered with sand deposits; and 3) Assessment of sand aggregate formation with oil in the presence of corrosion inhibitors.

Key words: Corrosion, Inhibition, Carbon dioxide, Carbon steel, solid particles

INTRODUCTION

Carbon steel used in combination with corrosion inhibitors is an economically favorable alternative for multiphase pipelines compared to the use of corrosion resistant materials. CO₂ corrosion inhibitor formulations contain surface-active compounds that form a protective layer at the pipe wall. The surfactants also adsorb to other surfaces and interfaces in the produced fluids, like solid particles and emulsion droplets, etc.¹⁻⁹

The solid particles may comprise sand and clay from the reservoir, and corrosion products and mineral scale. Fine solid particles, such as kaolinite clay, can consume a significant amount of corrosion inhibitor by adsorption.² This consumption may cause the inhibitor concentration to drop below the minimum effective concentration, and may lead to corrosion failure if the depletion of the inhibitor is not properly accounted for.³⁻⁴ Solids can affect detrimentally not only inhibitor performance, but many other aspects of the petroleum production as well. Sand particles are known to cause erosion corrosion. They can also deposit in some part of the pipelines or in separators, and cause severe attacks under the deposit.³ Corrosion inhibitor performance testing in presence of solids has received little attention so far.

¹ Present address: Det Norske Veritas, NO-1322, Høvik, Norway.

² Present address: Intecha, 170 00 Praha, Czech Republic.

³ Presenting author, e-mail: egil.gulbrandsen@ife.no

Copyright

The present paper describes parts of the results obtained in a recent joint industry project (see Acknowledgement section), where the objective was to develop test methods and test protocols for laboratory testing of CO₂ corrosion inhibitor performance. The paper focuses on the background and development of three methods for corrosion inhibitor testing in the presence of solids.

The first method is used to assess inhibitor performance in presence of suspended solids. The second method is used to test inhibitor performance under sand deposits. The third method is used to assess aggregation of sand and oil caused by presence of surface-active corrosion inhibitors.

The intention of the work was not to compare inhibitors. The inhibitors were used as example products in the development of the test method and identification of critical parameters for the testing. The presented test methods may also contribute to the development of improved inhibitor products.

TESTING OF INHIBITOR PERFORMANCE WITH SUSPENDED SOLIDS

This method was developed for screening tests of inhibitors and determination of the effective inhibitor concentration in the presence of suspended solids. The testing method is intended for field cases when solids are continuously produced in amounts that may reduce inhibitor performance. Kaolinite clay was used as a model solid with well-defined surface area.

Clay is added prior to inhibitor addition in the test method. This resembles the case where the solids are already present at the point of inhibitor injection. The effect of oil was also studied.

Experimental Procedure

All the tests were carried out in glass cells with a volume of 3 liters. Electrodes for electrochemical corrosion monitoring and pH measurements, temperature probes and gas inlets/outlets were inserted through stainless steel lids. The glass cell with accessories is schematically represented in Figure 1. A heating plate was used to control the temperature of the test solution, and the solution was gently stirred with a magnetic stirrer.

The test specimens were machined from X65 carbon steel. The element analysis and microstructure of the steel are given in Table 1. Cylinder specimens with surface area of 3.14 cm² were ground to 1000 mesh with wetted SiC paper prior to use. The specimens were wetted with isopropanol, cleaned with technical acetone in ultrasonic bath, and rinsed with ethanol. Then the specimens were blow dried prior to mounting on the specimen holders.

The test solutions were prepared from technical grade NaCl and distilled water. The pH was adjusted by addition of AR grade NaHCO₃. The test solutions were continuously purged with CO₂ grade 4.0. This gas contains less than 10 ppm of O₂, corresponding to less than 0.5 ppb dissolved in the solution in equilibrium with the gas at 1 bar and 25 °C.

The kaolinite clay was a reference clay, denoted KGa-2, from The Clay Mineral Society, University of Missouri, USA.⁹ The clay properties are given in Table 2. The surface area constituted by the clay is expressed in terms of surface area per unit volume of test brine (m^2/L). The standard kaolinite clay (KGa-2) has a specific surface area of $23.5 \text{ m}^2/\text{g}$. A clay concentration of 43 ppm therefore corresponds to an area of $1 \text{ m}^2/\text{L}$. A scanning electron image of the clay platelets, which were $0.1 \text{ }\mu\text{m}$ – $0.5 \text{ }\mu\text{m}$ thick and 0.5 – $2 \text{ }\mu\text{m}$ long, is shown in Figure 2.

The inhibitors used for the testing are listed in Table 3. The inhibitor concentrations are reported as ppm (i.e. mg/L) of blended product based on total liquid volume (water + oil).

The properties of the oils used in the tests are listed in Table 4; Oil 1 is a black oil, Oil 2 is a condensate, while Oil 3 is a refined, low-aromatic oil product. The oils were tested with Inhibitor M. Table 5 gives the partitioning of the inhibitor between the phases.

A potentiostat with a multiplexer was used for electrochemical measurements. The corrosion rate was monitored by the polarization resistance method (LPR) throughout the test. LPR measurements were performed in three-electrode configuration, i.e. working electrode - carbon steel specimen, reference electrode - Ag/AgCl , auxiliary electrode - Ti ring. The potential ramp for the LPR measurement was -5 mV to $+5 \text{ mV}$ vs. E_{cor} , with scan rate $0.1 \text{ mV}/\text{s}$. The corrosion currents was calculated as B/R_p . A constant value of $B = 20 \text{ mV}$ was used, based on polarization curves and mass loss determinations, as described in Refs. 13-14, and Appendix A. The corrosion rates are reported as average penetration rates ($1 \text{ A}/\text{m}^2$ corresponds to $1.16 \text{ mm}/\text{y}$). The polarization resistance was compensated for IR drop, determined by means of impedance spectroscopy (EIS). Potentiodynamic polarization curves were measured at the end of the test. The cathodic polarization curve was run from 0 to -250 mV vs. E_{cor} , and the anodic one from 0 to $+150 \text{ mV}$ vs. E_{cor} , both at scan rate $0.1 \text{ mV}/\text{s}$. All the specimens were inspected for localized attack by an optical microscope after the test.

The tests were carried out at $60 \text{ }^\circ\text{C}$, 0.8 bar CO_2 and pH 4.5. Most of the tests were performed in 10 % (w/w) NaCl brine. The solution in the glass cell was deoxygenated for 2-3 hours before the immersion of test specimens. Three specimens were introduced to each cell; two specimen for electrochemical measurements and one specimen for weigh loss measurements. The steel specimens were precorroded for 24 hours prior to addition of clay and inhibitor. Kaolinite clay was added to the cell 10 min before the inhibitor addition.

In the tests performed with 10 % oil, the oil was de-aerated with 1 bar CO_2 for minimum 4 hours and heated to test temperature before it was transferred to the test cell. 300 ml oil was transferred to the 3-litre test cell after start of precorrosion, and minimum 2 hours before the clay and inhibitor was introduced. A peristaltic pump was used to transfer the oil. The inhibitor was added to the cell from a 10 % stock solution, diluted with either oil or water.

Results and discussion

Inhibitor testing without oil. Examples of the experimental data from one test without kaolinite clay and one test with $2.5\text{ m}^2/\text{L}$ surface area of clay (108 ppm) are given in Figure 3. The baseline corrosion rate was approximately 3 mm/y. Kaolinite clay and 30 ppm of Inhibitor A was added after 24 hours of precorrosion. The inhibitor concentration was increased to 50 ppm towards the end of the test. The addition of the inhibitor resulted in a rapid decrease of the corrosion rate. The corrosion rate in the test with no clay continued to decrease until it stabilized at about 0.06 mm/y. The corrosion rate with clay stabilized at a higher corrosion rate (0.15 mm/y). This shows that the clay reduced the inhibitor performance.

Figure 4 summarizes the steady corrosion rates at the end of the tests, and residual concentrations of the active inhibitor compounds vs. the surface area of clay. The concentrations of the active compound given as the corresponding concentration of the formulated product. The residual analysis was carried out by the inhibitor suppliers. The corrosion rates are the steady corrosion rates for 30 ppm dose rate of the respective inhibitor.

The data for Inhibitor A illustrates a case when the inhibition effect was remarkably reduced in the presence of clay (Fig. 4a). The inhibited corrosion rate in absence of clay was 0.1 mm/y. The residual inhibitor concentration dropped to 11 ppm with $2.5\text{ m}^2/\text{L}$ clay surface area. Nevertheless the inhibited corrosion rate increased only slightly to 0.2 mm/y. With $5\text{ m}^2/\text{L}$ in the solution, the residual inhibitor concentration decreased to 5 ppm. This resulted in an increase of the corrosion rate to 0.4 mm/y. Only 2 ppm of Inhibitor A was left in the solution in the test with $7.5\text{ m}^2/\text{L}$ clay surface area (323 ppm clay). This depletion was associated with a dramatic rise of the corrosion rate to 2 mm/y, which was nearly the same as the uninhibited corrosion baseline. Similar results were obtained with Inhibitor B (not shown).

Figure 4b shows the results obtained with Inhibitor C. Even if the corrosion rate increased slightly with increasing clay concentration, the corrosion rate remained below 0.1 mm/y in presence of even in presence of $7.5\text{ m}^2/\text{L}$ clay surface area. The residual inhibitor concentration for this inhibitor was determined both for filtered and unfiltered solution sample. Despite some discrepancy between the results obtained with two analytical protocols, both of the data sets indicate that the inhibitor concentration was reduced to less than 20 ppm for $5\text{ m}^2/\text{L}$ of clay surface area. This shows that inhibitor performance in presence of suspended solids depends strongly on formulation.

The results of the tests with increasing dose of Inhibitor B are given in Figure 5. Two tests, one without clay and one with $5\text{ m}^2/\text{L}$ clay surface area, are shown in the figure. The corrosion rate decreased when 10 ppm of Inhibitor B was added for the test without clay. The corrosion rate continued to decrease with increasing amount of inhibitor until it stabilized when 80 ppm inhibitor was added. The inhibitor performance was negligible for 10 ppm of the inhibitor with $5\text{ m}^2/\text{L}$ of clay particle surface. With higher inhibitor concentrations the corrosion rate gradually decreased. Eventually at 150 ppm, the corrosion rate dropped to nearly the same value as for the test without clay. This indicates that it is possible to saturate the clay surface with inhibitor by adding sufficient amount of it, and in that way obtain adequate inhibitor performance.

Adsorption studies of surfactants on clay⁵ also showed that there was a limit concentration above which the adsorbed amount of the inhibitor did not increase, thus all the clay surface was saturated with the inhibitor. It was reported that zeta potential of kaolinite clay increased strongly with addition of CO₂ corrosion inhibitor, which contained cationic surfactant. Such behavior is consistent with adsorption of cations.^{2,4} Presence of other cations like Ca²⁺ can further reduce performance of cationic inhibitors.² On the other hand anionic inhibitors showed low affinity to clay.² The problem of parasitic consumption of inhibitor by clay and other fine particles in the produced fluids is a problem of determining and achieving the optimal dose rate. However, the chemistry of the inhibitor plays a key role in the problem. It appears possible to select an inhibitor product with acceptable performance in the presence of solids.

Inhibitor testing with oil present. A summary of the inhibitor test results with oil is given in Figure 6. All the experiments were carried out with 30 ppm of Inhibitor M. The corrosion rate generally increased with increasing clay concentration. In presence of clay, the corrosion rate for the tests with Oil 2 was lower than in the tests with the other oils, or those without oil. On the other hand, the corrosion rate with the other oils was higher than the corrosion rate without oil, for most the tests with clay present. The corrosion rate for Oil 1, and Oil 3 with 5 m²/L clay and more was nearly the same as the uninhibited baseline. These results indicate that oil can include components that may enhance or reduce the inhibitor performance, both in absence and presence of clay. The observed effects may rather be related to residual inhibitor concentration, than a direct interaction of oil and clay on the steel surface.

The specimen for one test with 10 % of Oil 3 got oil wetted, and the corrosion rate dropped to extremely low values. The oil-wetting phenomenon is not well understood yet; i.e. it is not possible to predict when oil wetting occurs.

Conclusions

- The inhibitor performance of some inhibitors was reduced in presence of clay due to adsorption. The test protocol allows distinguishing among different inhibitor product in terms of their sensitivity to clay.
- The sensitivity of the inhibitor performance to clay depends on the inhibitor chemistry. It appears feasible to formulate inhibitors so that the performance is little affected the present amounts of clay.
- For the inhibitors that were affected by the presence of clay, increased inhibitor dosage would efficiently saturate the clay surface and adequate inhibitor performance could be reached.
- Laboratory studies to select inhibitors should include experiments in the presence of representative solids at the expected concentration.

TESTS OF INHIBITOR PERFORMANCE UNDER SAND DEPOSITS

This test method was developed to evaluate CO₂ corrosion performance under sand deposits. The objective was to assess the risk of galvanic corrosion, formed due to sand

deposition on part of the steel surface, and to evaluate the ability of inhibitors to mitigate this type of corrosion.

The test method is intended for application with continuous sand production or with high probability of sand production. Sand deposition prior to inhibitor addition resembles the case of sand deposition under conditions of insufficient inhibition. Inhibitor addition prior to sand deposition represents the case of sand deposition under conditions of adequate inhibition (at least at bare surfaces). The effect of oil has not been included in the test method yet.

Experimental Procedure

The chemicals and specimen material were the same as described in the previous part of the paper, see Tables 1, 3 and 4. The tests were performed in 10 %(w/w) NaCl aqueous solution. Some tests were carried out at 60 °C, which correspond to CO₂ partial pressure of 0.8 bar. Other tests were performed at 90 °C with CO₂ partial pressure 0.5 bar.

The sand used in these tests was analytical grade, acid-washed and calcinated silica sand. The grain size was specified as 200-400 mesh (30-80 micron). However, in-house SEM examination showed particle diameters of 200–600 μm (Figure 7). Estimating by use of a sphere model, the geometric area was less than 0.01 m²/g. Surface area measurements by the BET technique (nitrogen adsorption) indicated ca. 0.1 m²/g, which indicated substantial porosity and roughness of the sand grains. This is to some extent supported by the SEM image. The sand layer thickness was about 5 mm in all tests. The total amount of sand in the cell was approximately 3 g. The sand thus had a total surface area of about 0.3 m².

The test set-up is shown in Figure 8. A specimen assembly consisting of three specimens used in most of the tests; one specimen not covered by sand (abbreviated NS - no sand), and two specimens fully covered by sand (abbreviated as FS1 and FS2 - fully sand covered). Specimens FS1 and NS were galvanically coupled, while the FS2 specimen was not galvanically coupled to other specimens. The area of the NS specimen was ca. 4 cm², while the areas of each of the FS specimens were 1 cm². The specimens were molded into epoxy, and pretreated as described in the previous part of this paper. The sand was deposited with negligible air ingress by means of a specially designed glass tube device. The sand was contained between two moveable pistons. In the tests with inhibitor added before the sand, the sand was saturated with inhibitor by flushing with portions of the inhibitor containing test solution.

The FS1 and NS specimens were galvanically coupled by means of the ZRA (Zero Resistance Ammeter) facility of the potentiostat. The galvanic current was logged at regular intervals. The corrosion current was measured with the polarization resistance technique in the galvanically coupled mode, with individual ZRA current measurement on each specimen of the couple. The potential was scanned from -5 mV to +5 mV vs. E_{oc} of the couple, at a scan rate of 0.1 mV/s. The anodic dissolution current calculation is described in Appendix A.

The tests were performed in two different ways. The sand was deposited 1-3 days prior to inhibitor addition in the test resembling the case of sand deposition under conditions of insufficient inhibition. In the test resembling the case of sand deposition under conditions

of adequate inhibition, the inhibitor was introduced 1-2 days before sand was deposited on the steel surface. The sand surface was then saturated with inhibitor by exposure to portions of the inhibited brine before deposition on the specimen surface.

Results

Sand deposited before inhibitor addition. The results for a test where sand was added before Inhibitor C are shown in Figure 9. Only NS and FS1 were exposed in this initial test. The baseline corrosion rate without sand was about 2 mm/y. Sand was added 6 hours after specimen immersion. After one day exposure 30 ppm inhibitor C was added. The corrosion rate of the NS specimen (not covered by sand) decreased rapidly due to the inhibition effect of Inhibitor C. The steady corrosion rate for the NS specimen was 0.03 mm/y. The corrosion rate of the FS specimen decreased gradually to about 0.5 mm/y. Increasing the inhibitor concentration to 50 ppm did not have significant effect on the corrosion rates.

Sand deposition caused increasing galvanic current between the FS1 and NS specimen (Fig. 9b). FS1 was the anodic part of the couple. The galvanic current continued to increase after inhibitor addition. It reached a maximum of 0.3 A/m^2 ten hours after inhibitor injection. Then the galvanic current decreased slowly.

The mixed corrosion potential of the galvanic couple vs. Ag/AgCl reference electrode is given in Figure 9c. The uninhibited corrosion potential without sand was -665 mV . The corrosion potential increased during the precorrosion time, which is usually observed during precorrosion of the specimens. The corrosion potential increased further when inhibitor was added to the cell. This is in agreement with the literature data on the kinetics of inhibition of CO_2 corrosion.¹⁰⁻¹¹ It was reported that the first step in the inhibition process was the inhibitor adsorption on the steel surface. The adsorption step was associated with an increase in the corrosion potential of the steel.¹⁰⁻¹¹ For the present test, addition of the inhibitor resulted in an immediate increase of the potential on the specimen directly exposed to the brine (NS). The corrosion potential of NS specimen increased faster than the corrosion potential of the sand covered specimen (FS1); probably due to slow mass transport of inhibitor through the sand layer. This was a systematic trend in all experiments. The FS1 specimen accordingly became anodically polarized, leading to galvanic corrosion. Examination of the surfaces showed general corrosion at the NS specimen (Fig. 9d). The FS1 specimen had a rougher surface than the NS one, but no localized corrosion was found.

The results for a test where sand was added before Inhibitor J are given in Figure 10. Sand was added 6 hours after specimen immersion, and 50 ppm of Inhibitor J was added 25 hours later. The uninhibited baseline corrosion rate of the non-coupled sand covered specimen (FS2) was about 1 mm/y (Fig. 10a). When inhibitor was added to the solution the corrosion rate of the (uncoupled) FS2 specimen was reduced to 0.1 mm/y. The corrosion rate of the NS specimen decreased to 0.2 mm/y. The LPR corrosion rate on the FS1 specimen (with sand and galvanically coupled to NS) on the other hand, increased straight after the inhibitor addition and reached a maximum of nearly 3 mm/y before it slowly decreased to 0.3 mm/y where it stabilized. The fast inhibition of the uncoupled FS2 specimen indicates that the inhibitor reached the specimen surface relatively fast. The

corrosion rate under the sand deposit was mitigated by the inhibitor with time, even for the galvanically coupled FS1 specimen.

Figure 10b shows that the inhibitor addition resulted in an instantaneous increase of the galvanic current density on the FS1 specimen. The current slowly decreased with time and stabilized at about 0.2 A/m^2 . The substantial part of the increased corrosion rate was caused by the galvanic effect (An anodic current density of 1 A/m^2 corresponds to a penetration rate of 1.16 mm/y).

Photographs of the specimens after the test are shown in Figure 10c. Two wide pits were found on the FS1 specimen, approx. $340 \mu\text{m}$ and $420 \mu\text{m}$ deep ($\sim 4\text{-}5 \text{ mm/y}$ in average penetration rate). Signs of localized attack was also found on the FS2 specimens, $220 \mu\text{m}$ ($\sim 3 \text{ mm/y}$) deep. No localized attack was observed on the NS specimens.

Inhibitor added before sand deposition. The results of a test with Inhibitor A at 90°C are shown in Figure 11. The inhibitor was added after 2 hours of precorrosion. The LPR corrosion rate for all specimens was reduced to less than 0.2 mm/y when 50 ppm Inhibitor A was added to the cell (Fig. 11a). Sand was added after 2 days of exposure. The corrosion rate of the FS1 specimen (galvanic coupled to the NS) was increasing gradually during the entire test. It went up to nearly 3 mm/y at the end of the test. The corrosion rate of the FS2 specimen (sand covered, not galvanically coupled) reached a stable value of 0.1 mm/y within few days after inhibition addition. The corrosion rate of the NS specimen increased slowly from 0.2 mm/y to 0.5 mm/y during exposure. Increasing the inhibitor concentration to 100 ppm for the few last days did not have any effect on the corrosion rate. The galvanic current increased with time. Figure 11b shows that a substantial part of the increased corrosion rate on the FS1 specimen was caused by the galvanic effect.

Inspection of the surface of the FS1 specimen showed severe general corrosion attack over the entire surface with depth of $100\text{-}330 \mu\text{m}$ (Fig. 11c). The corrosion attack was deepest in the part of the surface that was closest to the NS specimen. The specimen NS had experienced crevice attacks at the edge of the specimen. It was difficult to remove the corrosion products in the crevice, and therefore it was difficult to estimate the depth of the attack. The deepest measurable attack was $180 \mu\text{m}$ deep, which corresponds to a local corrosion rate of 1.2 mm/y . The FS2 specimen was very little corroded.

Figure 12 shows the results of a test where Inhibitor J was added before sand deposition. The specimens were precorroded for 20 hours before inhibitor J was added, and the sand was added after two days exposure. The corrosion rate for all the specimens decreased rapidly after inhibitor was added to the cell (Fig. 12a). The corrosion rates were nearly the same for all the specimens, about 0.1 mm/y . The corrosion rates stayed stable during the entire experiment. The galvanic density of the specimen FS1 became anodic when sand was deposited on the specimen (Fig. 12b). The anodic current density then decreased from 0.1 A/m^2 to 0.04 A/m^2 . There was a wide edge attack found on the FS1 specimen with a depth of $800 \mu\text{m}$, in addition to several pits from 20 to $70 \mu\text{m}$ deep. Small pits with depth about $20 \mu\text{m}$ were found on the FS2 specimen. Few pits with the same depth were also observed on the NS specimen. There were also edge attacks up to $230 \mu\text{m}$ deep on the NS specimen. These were not as wide as the edge attack on the FS1 specimen.

Discussion

Generally, the experimental work with test of inhibitor performance under sand deposits showed that the sand deposition resulted in a potential difference between the sand covered specimens (FS) and the specimen exposed directly to the brine (NS). The sand covered specimen become anodically polarized with the specimens coupled. The galvanic effect might also cause severe localized corrosion attacks on the sand covered specimen (FS). The galvanic corrosion attack occurred both when sand was added before inhibitor (resembles the case of sand deposition under conditions of insufficient inhibition) and when the inhibitor was added before the sand (resemble the case of sand deposition under conditions of adequate inhibition). The localized attack on the sand covered specimen was more severe when the sand was added before the inhibitor. In this case the sand probably adsorbed a large amount of the inhibitor at the same time as the sand provided a barrier against the mass transfer of the inhibitor molecules through the sand layer. This resulted in an under-dosage of the inhibitor on the steel surface covered by sand and could lead to a development of localized attack, also on a sand covered specimen without galvanic coupling to other specimens.

Four factors were identified as important regarding the galvanic corrosion problem under sand deposits:

1. The potential difference between FS and NS specimen
2. The solution resistance and the polarization resistance of the NS specimen
3. Transportation of inhibitor through the sand layer
4. Environmental changes under sand

The potential difference between the uncoupled specimens was the driving force for the galvanic current of the galvanically coupled specimens. Larger difference between the respective open circuit potentials of the FS and NS specimen would result in greater anodic polarization of the FS specimen, and in greater susceptibility to galvanic corrosion. The potential difference was likely to be different for various inhibitors.

The polarization resistance, R_p , of the NS specimen might be the limiting resistance for the galvanic current flow in the tests. It should be kept in mind that the corrosion rate is inversely proportional to R_p . This suggests that the FS1 specimen should be better protected against galvanic corrosion the lower the corrosion rate was on the NS specimen (other factors being the same). Initiation of localized corrosion would also decrease the polarization resistance of the sand covered specimen and hence it would increase the current flow (and lead to even larger increase of the current density in the localized attack). It is therefore essential to avoid pitting corrosion.

Adsorption of the inhibitor onto the sand may deplete inhibitor from the solution inside the sand layer. The high ratio of sand surface area to liquid volume inside the sand layer (order of 300 m²/liter) show that the test procedure must include a step to saturate the sand with inhibitor from a large volume of solution before it is deposited onto the specimens, as done in the present tests.

High pH and high content of iron ions would be favorable for iron carbonate precipitation on the surface of FS specimen. Iron carbonate precipitation may reduce the corrosion rate

under the sand layer before the inhibitor was transported to the steel surface, but it might also contribute to the localized nature of the attack under the sand. If the corrosion film deposited only on parts of the surface, this may result in localized corrosion.

Conclusions

- Sand deposition resulted in a potential difference between the sand covered specimens (FS) and the specimen exposed directly to the brine (NS). The sand covered specimen became anodically polarized in presence of inhibitor. The galvanic effect might cause severe localized corrosion attacks on the sand covered specimen (FS).
- The galvanic corrosion attack occurred both when sand was added before inhibitor and when inhibitor was added before the sand. However, it appears possible to formulate inhibitors that reduce the corrosion rate to an acceptable level. The test method appears capable to differentiate between the inhibitors.
- Evaluation of the susceptibility to pitting corrosion is one of the key issues in the test method. Factors that can increase the susceptibility to localized corrosion with inhibition include anodic polarization, under-dosage of the inhibitor, degradation of the inhibitor with time at higher temperatures, and corrosion product layer formation.

SAND AGGREGATION TEST

During the testing with kaolinite clay, a sand aggregation phenomenon was observed in a system containing sand, oil and inhibitor. Sand aggregation can result in challenges for transportation and processing of the oil. Tests with several inhibitors were carried out to delineate this aggregation phenomenon. The test method was developed to assess the tendency of corrosion inhibitors to cause the aggregation of produced sand. The test method is intended for application with continuous sand production or with high probability of sand production.

Experimental Procedure

The chemicals are the same as described in the previous parts of the paper. The overview of the inhibitors used for the tests are given in Table 3. The tests were carried out in a glass cells at 60 °C, 0.8 bar CO₂, pH 4.5 in 10 %(w/w) NaCl brine with and without Oil 3 (Table 4). After the solution in the cell was purged with CO₂ for at least 4 hours, 100 g of sand was added to the cell. The solution with sand was stirred for 15 min, before the inhibitor was added to the cell.

The evaluation of the tests was based on visual observations of tendency of sand grains to form larger aggregates. Strong, some or no occurrence of the following tendencies was reported: tendency to aggregate; cake formation; sticking to walls; and buoyancy of the aggregates.

Results

The initial testing showed that the sand aggregate formation only occurred when both oil and inhibitor was present. Visual observations, like the pronounced buoyancy of some

aggregates, indicated that the aggregates contained oil. Figure 13 shows photos from a test with Inhibitor M and 1 % of Oil 3. Even at such low oil concentration, sand aggregation occurred at 5 ppm of the inhibitor. Cake formation and sticking of sand to the walls was observed at 10 ppm of Inhibitor M.

Figure 14 shows photos from the test with Inhibitor N and 10 % of Oil 3. The sand aggregation was observed for concentration higher than 5 ppm of Inhibitor N. The sand aggregates did not stick to the wall, and no cake formation was observed at higher concentration. The aggregates became more buoyant instead. The appearance of the aggregates seemed to be a combination of oil properties and inhibitor chemistry, but no general trends have so far been revealed.

Discussion

This phenomenon has recently been studied in more detail using a generic inhibitor compound, see ref. 7. It was concluded that the inhibitor changed the wettability of the sand surface from hydrophilic to intermediate wettability. Intermediate wettability is known as a favorable condition for the formation of particle stabilized emulsions.¹² Based on a comparison with such emulsions, it was suggested that an oil stabilized sand aggregate was formed, rather than an oil-in-water emulsion, due to the great size of the sand grains.

Conclusion

- Sand aggregation occurred only in presence of both oil and inhibitor. However only very small quantities of oil and inhibitor were needed to start the aggregation of the sand. The aggregation behavior depended somewhat on the sample of oil and the inhibitor.

ACKNOWLEDGEMENT

The work was carried out in the joint industry project “Kjeller Inhibitor Project – Phase II” funded by ChevronTexaco, Clariant, ConocoPhillips, ENI Agip, M-I Production Chemicals, Nalco, Norsk Hydro, Saudi Aramco, Statoil, and Total.

REFERENCES

1. D.F. Evans, H. Wennerström, *The Colloidal Domain*, 7, Wiley-VCH, Inc. (1994).
2. E. Gulbrandsen, J. Kvarekvål, A. Dugstad, EUROCORR 2003, Paper no. 177, European Federation of Corrosion, Budapest, Hungary (2003).
3. J.P. Smith, I.A. Gilbert, R.W. Kidder, Syamsudin, in *Corrosion/2001*, Paper No.29, Houston, TX: NACE International, (2001).
4. E. Gulbrandsen, J. Kvarekvål, Proc. 16th International Corrosion Congress, Paper no. 4-40, International Corrosion Council, Beijing, China (2005).
5. J.Wang et al., *J. Colloid and Interface Sci.*, 213, 596 (1999).
6. R. Atkin, V.S.J Craig., E.J. Wanless, S. Biggs, *Advances in Colloid and Interface Science* 103, 219 (2003).

7. E. Gulbrandsen, A. Pedersen, Proc. 2007 SPE International Symposium on Oilfield Chemistry, paper no. SPE 106492, Society of Petroleum Engineers, Richardson, TX.
8. D.F. Evans, H. Wennerström, The Colloidal Domain, 67, Wiley-VCH, Inc. (1994).
9. H. van Olphen and J. Fripiat (ed.), "Data Handbook for Clay Minerals and other Non-Metallic Minerals", Pergamon (1979).
10. K. Bilkova, E. Gulbrandsen, M. Knag, J. Sjöblom, Proceedings of the 10th European Symposium on Corrosion and Scale Inhibitors (10 SEIC), Ann. Univ. Ferrara, N.S., Sez. V, Suppl. N. 12, 585, 2005. Ferrara, Italy (2005).
11. K. Bilkova, E. Gulbrandsen, Submitted to Electrochimica Acta
12. R. Aveyard, B. Binks, J.H. Clint, Advances in Colloid and Interface Science 100-102, 535 (2003).
13. E. Gulbrandsen, J. Kvarekvål, H. Miland, "Effect of Oxygen Contamination on Inhibition Studies in CO₂ Corrosion", Corrosion, 61, 1086 (2005).
14. E. Gulbrandsen, A. Granå, "Testing of CO₂ corrosion inhibitor performance at high flow velocities in jet impingement geometry. Effects of mass transfer and flow forces.", Corrosion, 63, 1009 (2007).

Table 1. Element analysis (%w/w) and steel microstructure

Steel	Designation	Microstructure
X-65 carbon steel	API 5L X65	Ferritic-pearlitic

Steel	C	Si	Mn	S	P	Cr	Ni	V	Mo	Cu	Al	Sn	Ti	Nb
X-65	0.08	0.25	1.54	0.001	0.019	0.04	0.03	0.045	0.01	0.02	0.038	0.001	0.002	0.043

Table 2 Properties of Kga-2 kaolinite clay from Clay Mineral Society.⁹

Cation exchange capacity 3,3 meq/100g											
Surface area N ₂ area: 23,50 ± 0,06 m ² /g											
Chemical composition (%):											
SiO ₂	Al ₂ O ₃	TiO ₂	Fe ₂ O ₃	FeO	MnO	MgO	CaO	Na ₂ O	K ₂ O	P ₂ O ₅	S
43,9	38,5	2,08	0,98	0,15	n.d.	0,03	n.d.	<0.005	0,065	0,045	0,02

Table 3 List of inhibitor products tested in the project. Data extracted from MSDS and supplier information

Inhibitor	Actives	Preferential solubility
A	Alkyl amino acid	
B	Quaternary ammonium salt, amino fatty acids	
C	Imidazoline, betaine, amine ethoxylate	Water soluble
J	Imidazoline salt	
M	Polyamine	Insoluble (dispersible)
N	Quaternary ammonium salt	Miscible in all proportions

Table 4 Available data for the oils used in the tests.

Parameter/element	Units	Oil 1	Oil 2	Oil 3
Density (15 °C)	Kg/litre	0.83	0.77	0.788
Water	Mass %	0.007	0.008	< 0.005
Acid number	mg KOH / g	0.08	0.08	-
Sulphur	mg / kg	1020	500	< 1
Nitrogen	mg / kg	600	200	-
SARA*:				
Saturates	mass %	71.2	84.4	93.3
Aromatics	mass %	25.0	12.7	0.0
Polar comp.	mass %	2.6	2.3	6.3
Asphaltenes	mass %	1.2	0.6	0.5
Hydrocarbons	mass %	96.2	97.1	93.3
NSO	mass %	3.8	2.9	6.8

*SARA: Saturates-Aromatics-Resins-Asphaltenes. Analytical Protocol: NIGOGA, 4th Edition (The Norwegian Industry Guide to Organic Geochemical Analyses)

Table 5 Partitioning behavior of Inhibitor M between oil, water and clay in fluids from bubble tests. Data provided by the supplier.

Oil used	In oil [%]	In brine [%]	At clay surface [%]
Oil 1	4	36	60
Oil 2	5	45	50
Oil 3	5	48	47

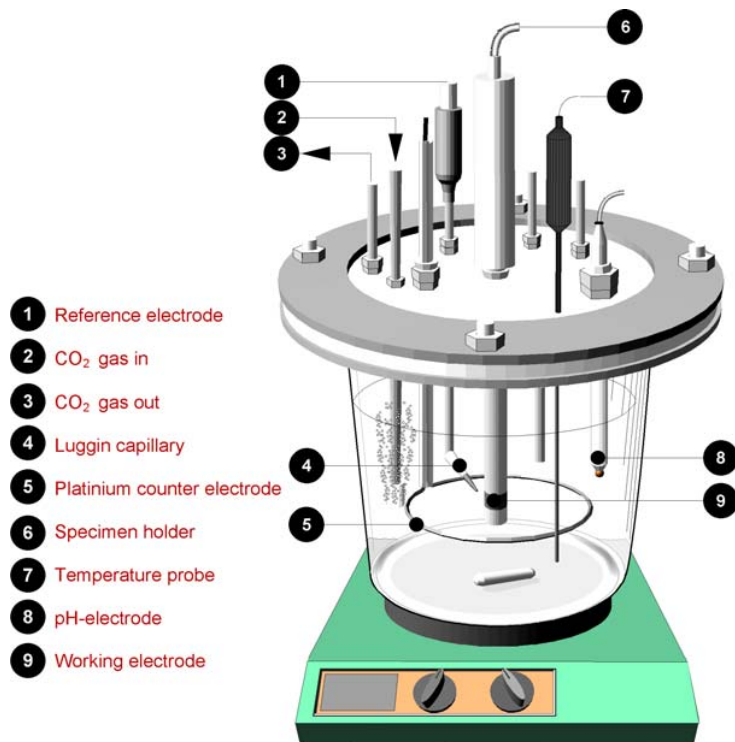


Figure 1 Glass cell with accessories. The actual counter electrode was made of titanium.



Figure 2 SEM image of KGa-2 kaolinite clay from Clay Mineral Society.⁹ The clay flakes are 0.1-0.5 μm thick and 0.5-1 μm long.

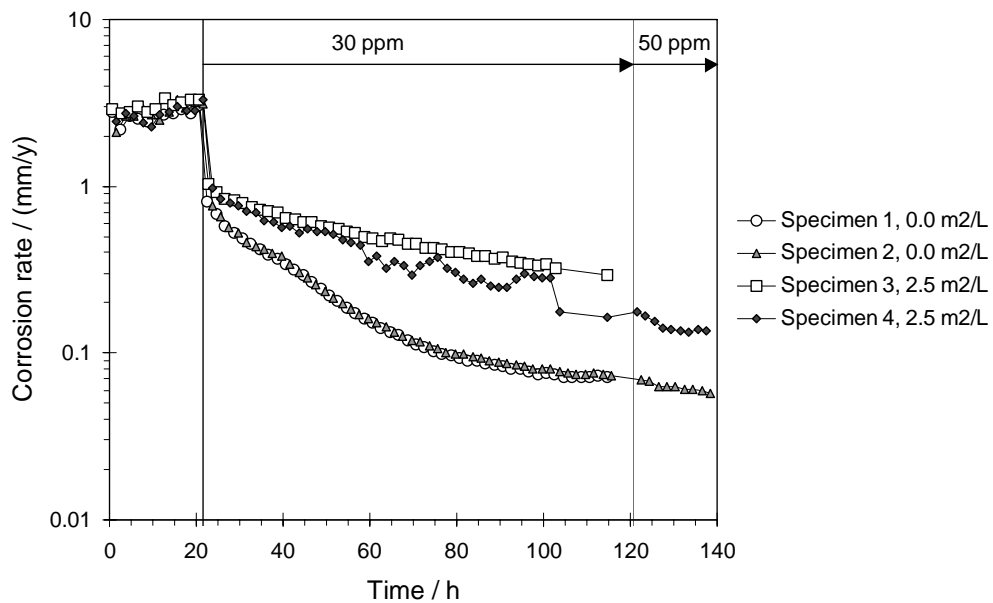
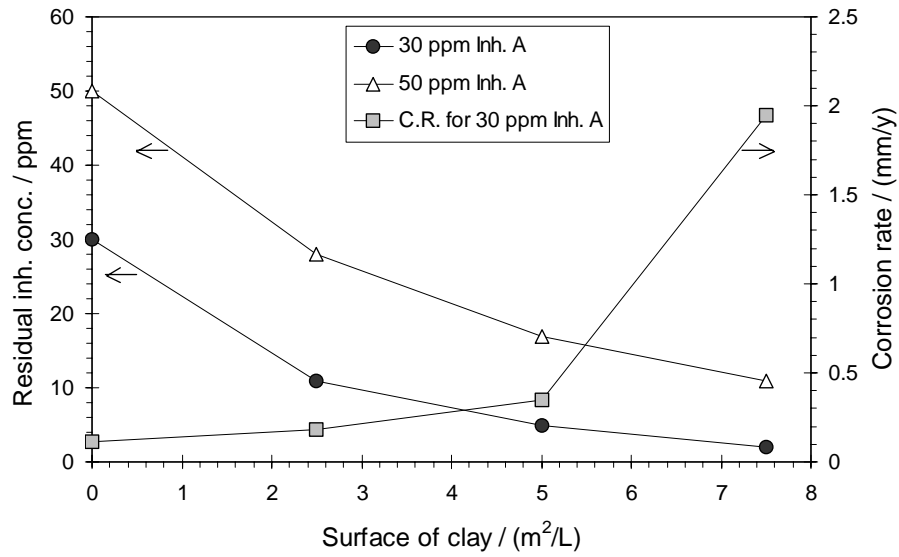
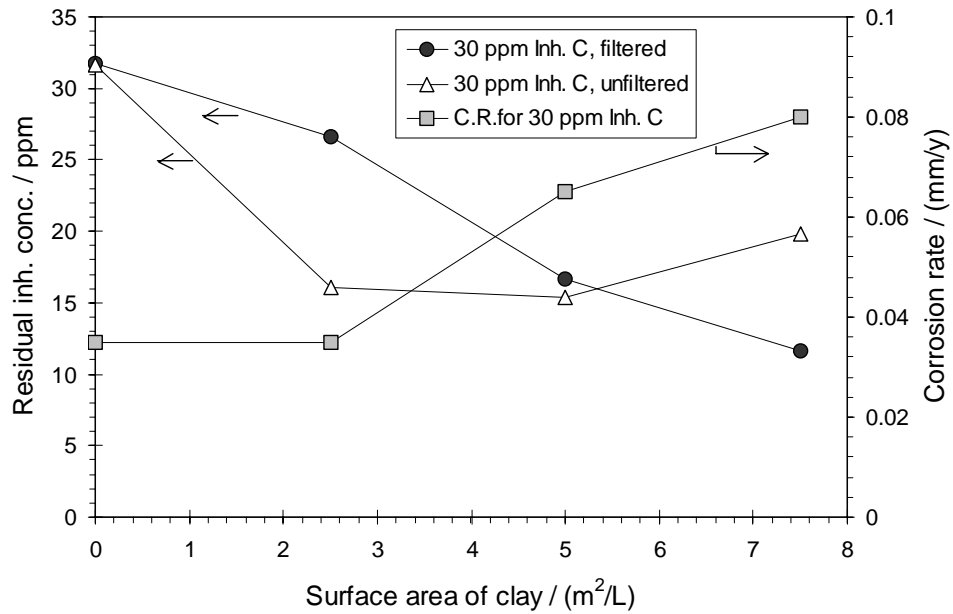


Figure 3 Example of the experimental data. LPR corrosion rate vs. time at clay concentrations 0.0 and 2.5 m^2/L . Test conditions: 60 °C, 0.8 bar CO_2 , pH 4.5, 10 % NaCl, Inhibitor A. Clay added 10 min before the inhibitor.



a)



b)

Figure 4 Residual inhibitor concentration (left axis) and inhibited corrosion rate (right axis) vs. kaolinite clay surface area. a) Inhibitor A, b) Inhibitor C. Test conditions: 60 °C, 0.8 bar CO₂, pH 4.5, 10 % NaCl, inhibitor concentration for the corrosion test: 30 ppm. Residual analysis was carried out by the suppliers of the products.

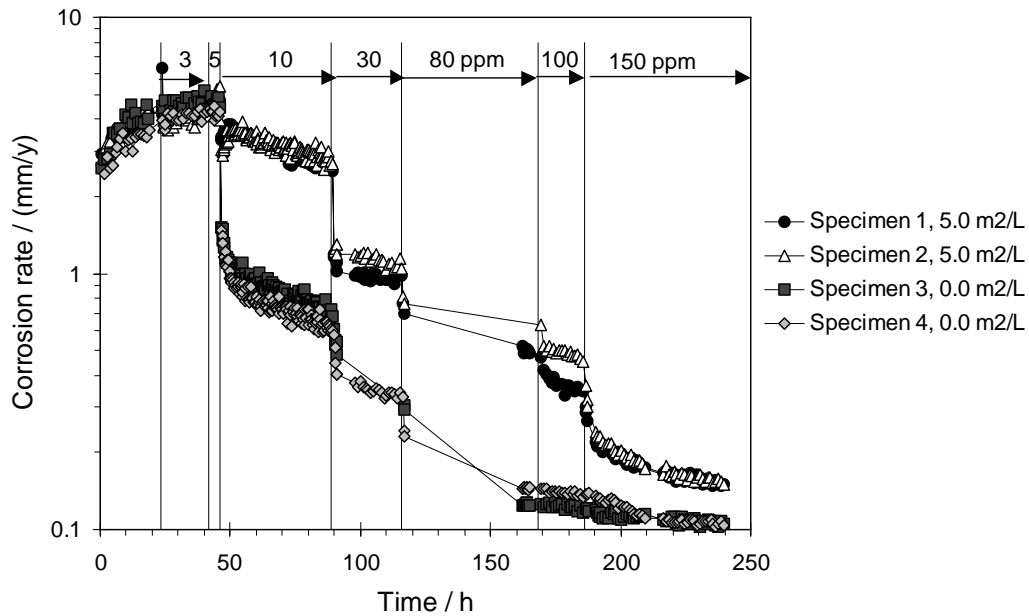


Figure 5 LPR corrosion rate vs. time in test with precorroded specimen and stepwise addition of inhibitor B. Test conditions: 60 °C, 0.8 bar CO₂, pH 4.5, 10 % NaCl.

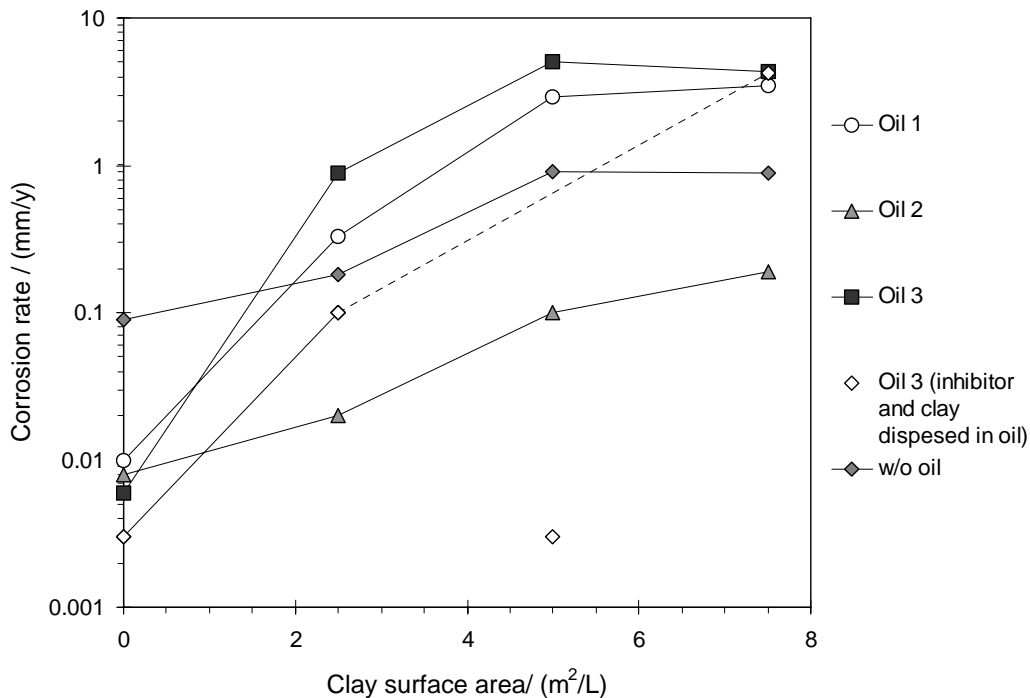


Figure 6 Summary of the final, inhibited corrosion rate vs. clay surface area in the different corrosion tests performed with 10 % oil and 30 ppm Inh. M. Tests with Oil 1, 2 and 3 where clay and inhibitor were dispersed and diluted in distilled water and a test with Oil 3 where clay and inhibitor was dispersed and diluted in Oil 3.

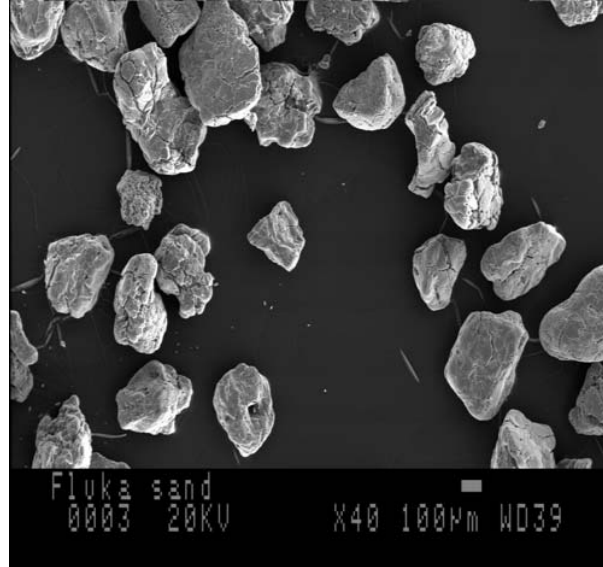


Figure 7 SEM image of the calcinated acid washed silica sand. Particle diameters of the sand are 200-600 μm .

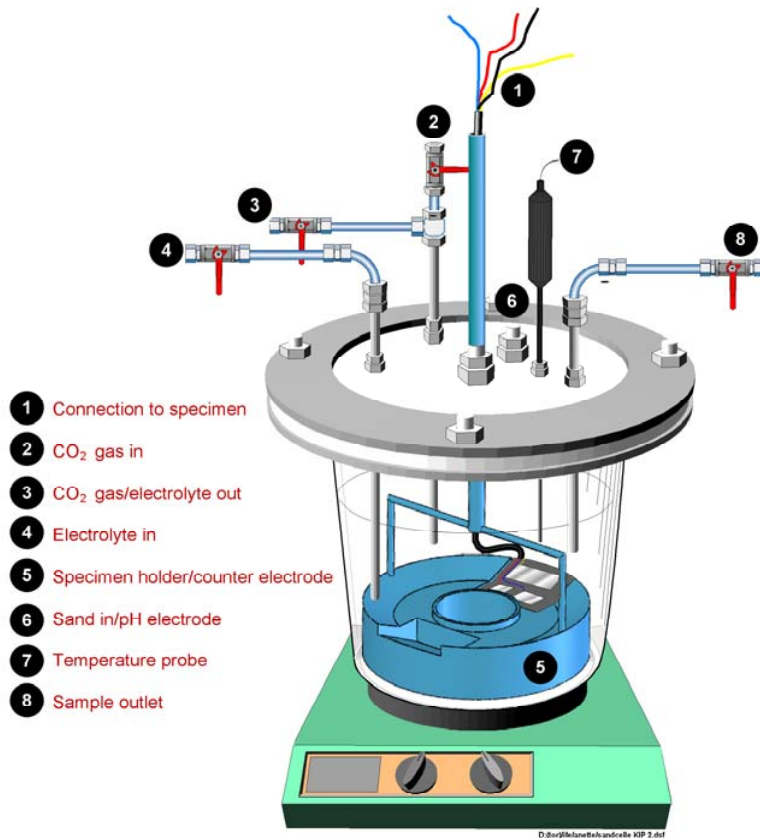
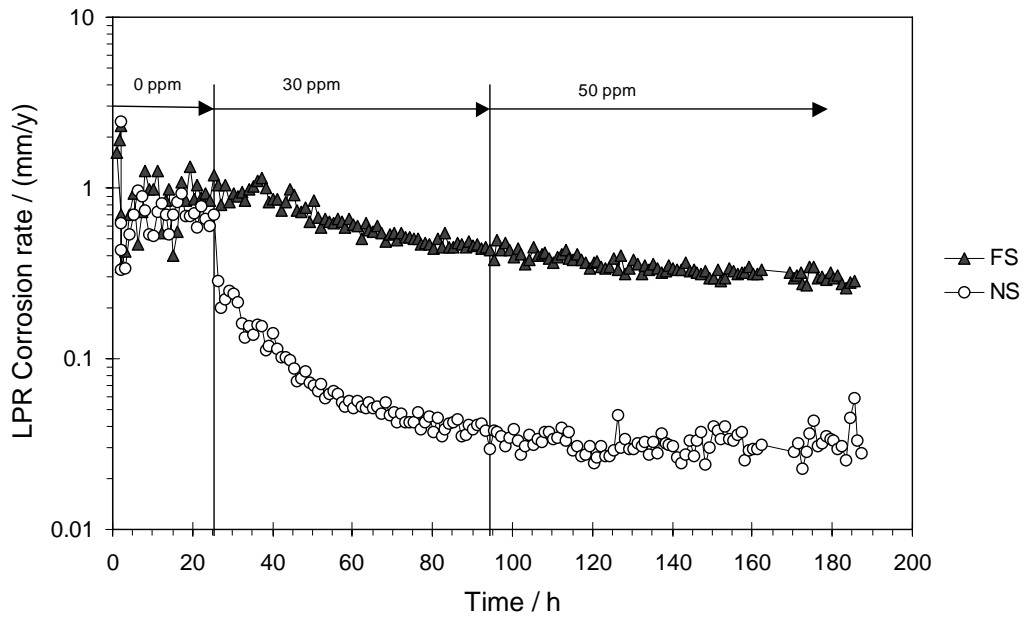
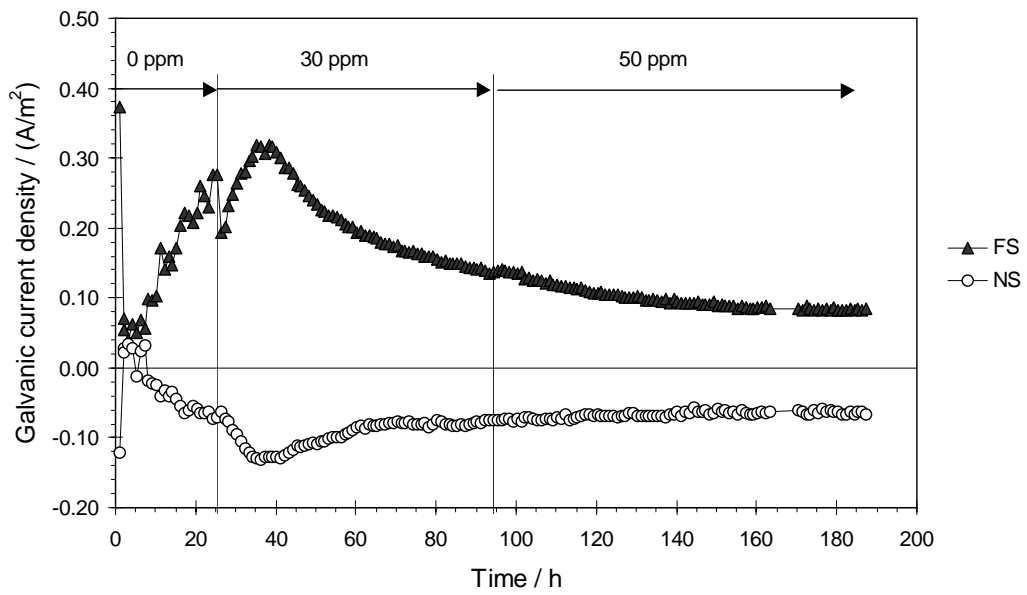


Figure 8 Glass cell equipped with specimen holder assembly for inhibitor performance testing under sand deposits.

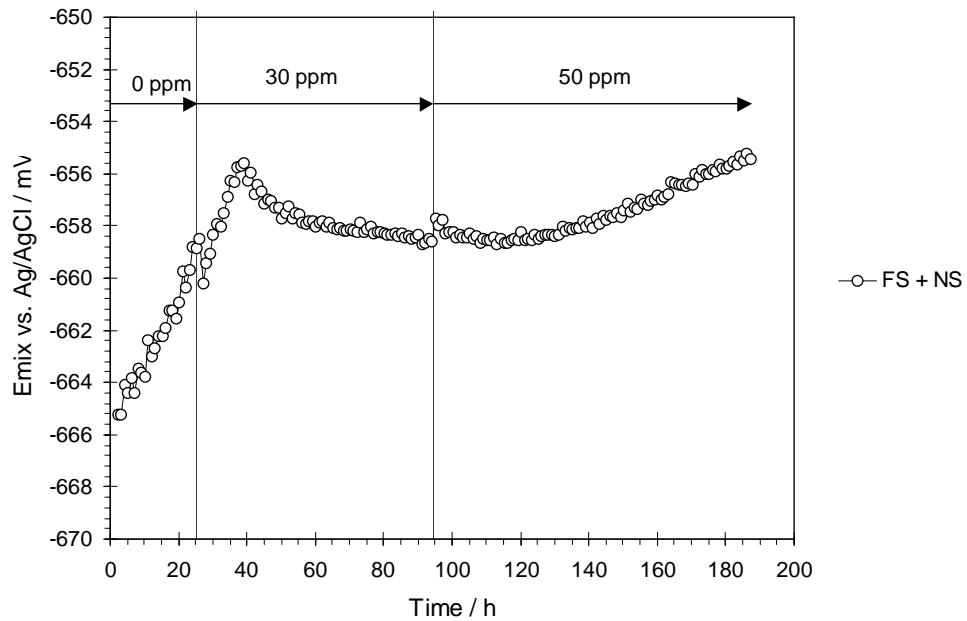


a)

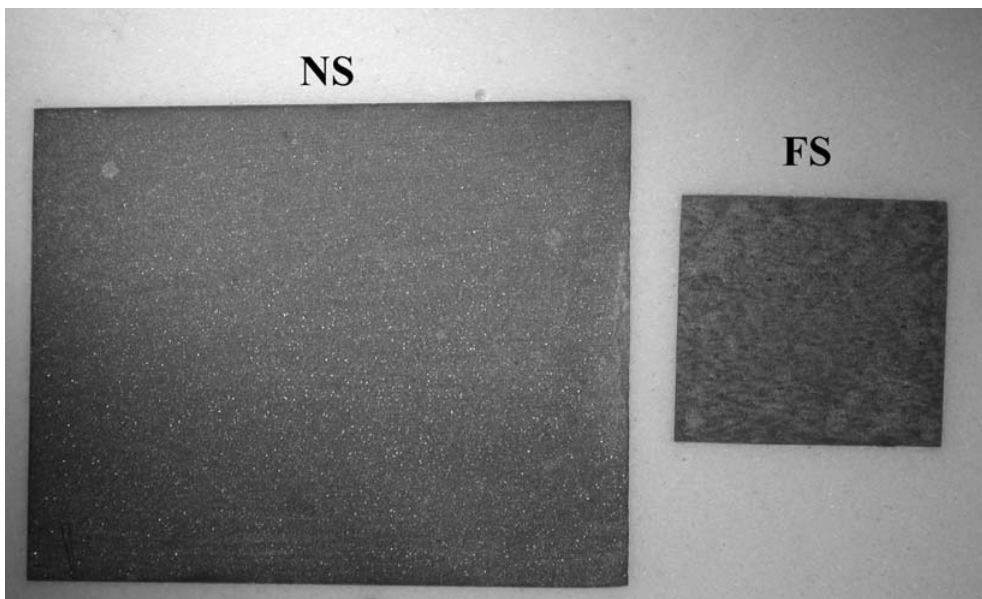


b)

Figure 9a-b Caption overleaf

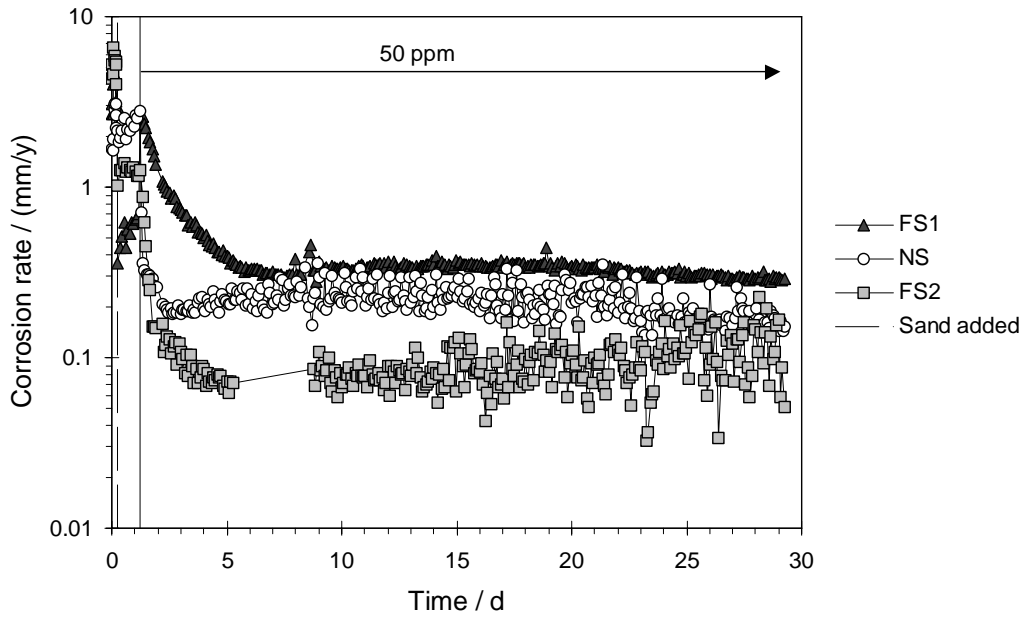


c)

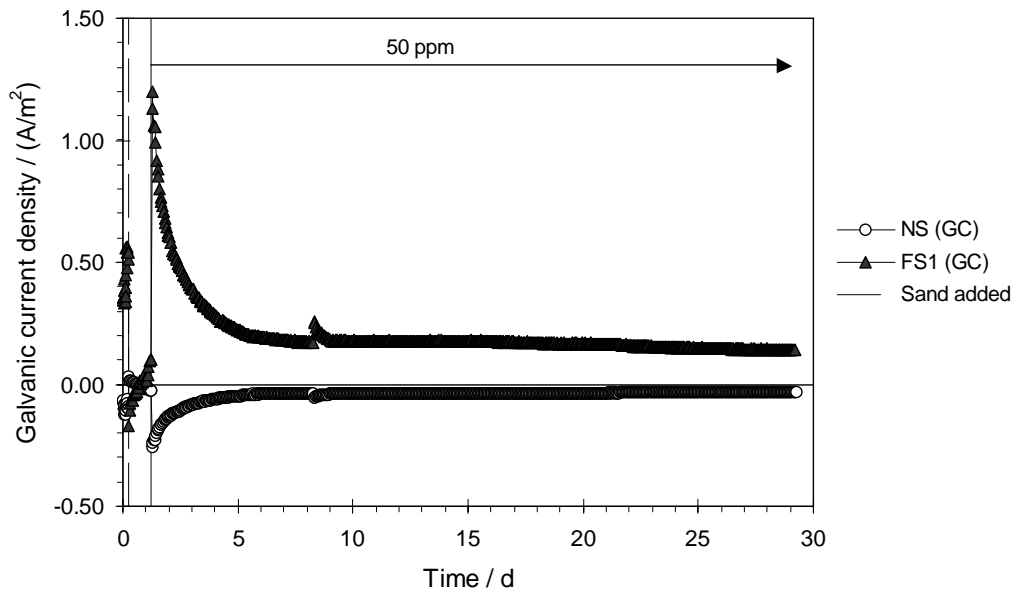


d)

Figure 9 Results of the test when sand was added before Inhibitor C. a) LPR corrosion rate of the galvanically coupled specimens. b) Galvanic current density of the specimens. c) Corrosion potential of the coupled specimens (FS + NS) vs. Ag/AgCl reference. d) Photos of the specimens after exposure. Test conditions, 10 % NaCl, 60 °C, pH 4.5, 0.8 bar CO₂, 30 - 50 ppm Inhibitor C.



a)



b)

Figure 10 a-b Caption overleaf

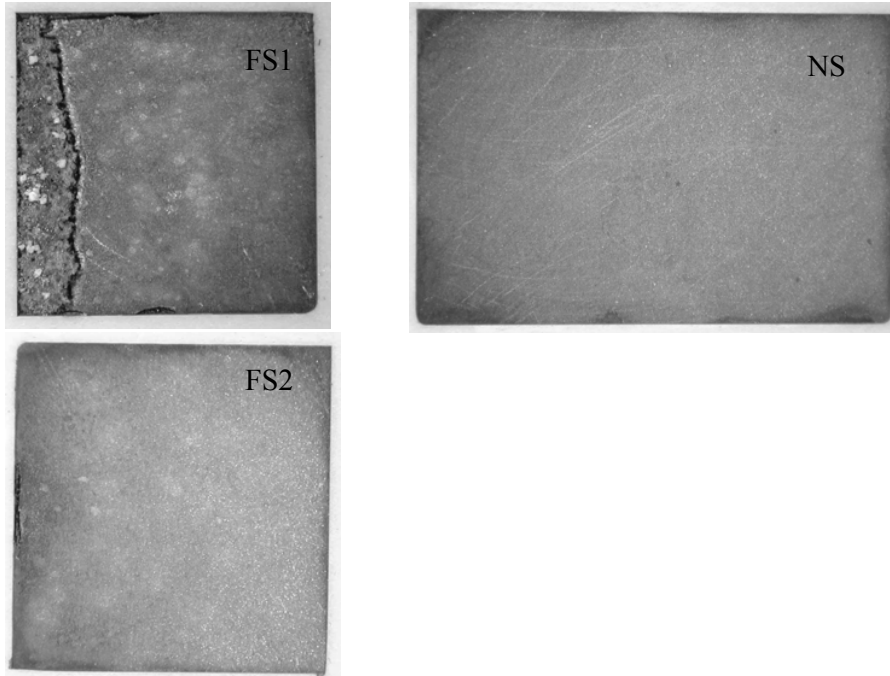
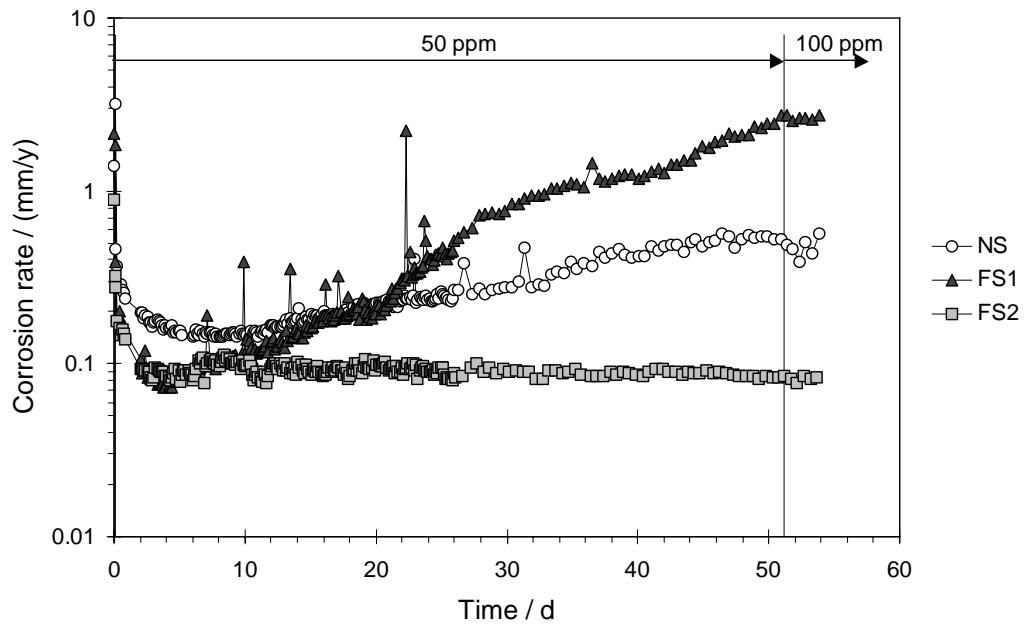
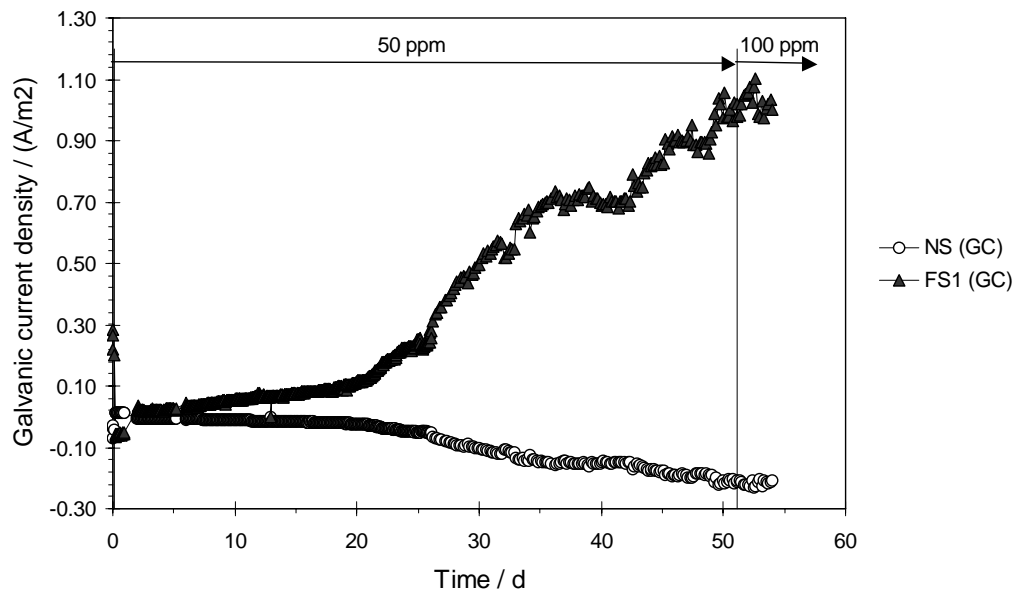


Figure 10 Results of the test when sand was added before Inhibitor J. a) LPR corrosion rate. b) Galvanic current density of the specimens. c) Photos of the specimens after exposure. Test conditions, 10 % NaCl, 60 °C, pH 4.5, 0.8 bar CO₂, 50 ppm Inhibitor J.

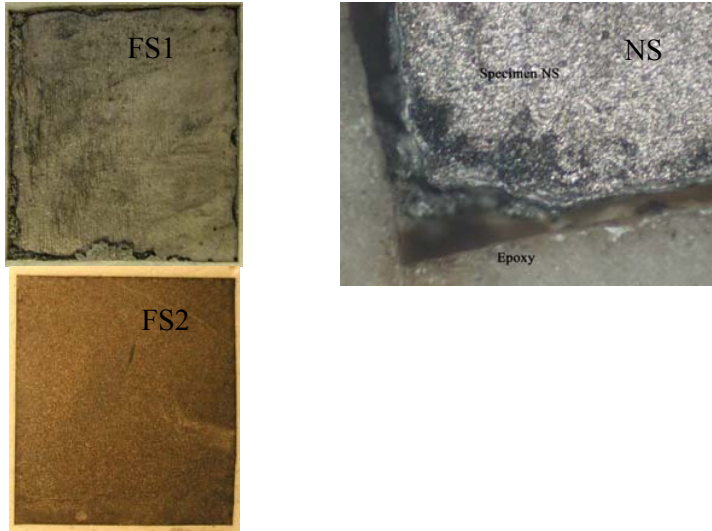


a)



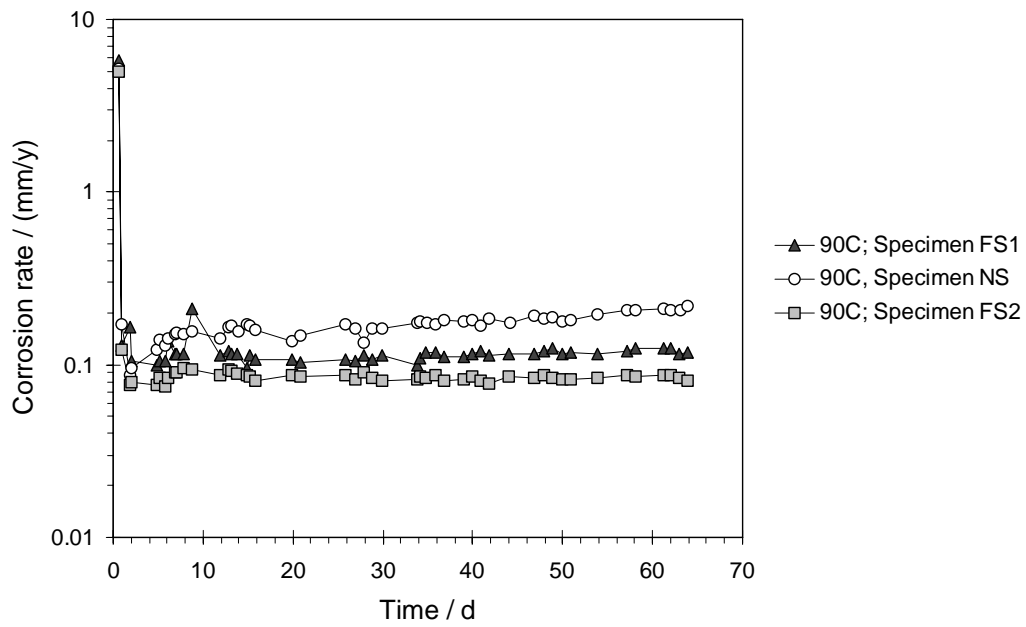
b)

Figure 11a-b Caption overleaf



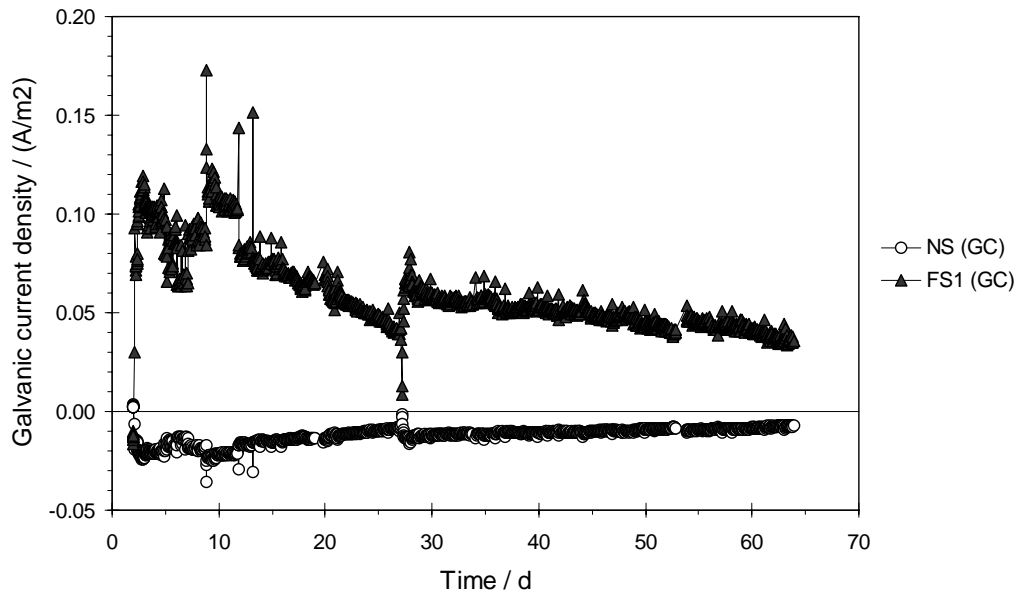
c)

Figure 11 Results of the test when Inhibitor A was added before sand. a) LPR corrosion rate. b) Galvanic current density of the specimens. c) Photos of the specimens after exposure. Test conditions, 10 % NaCl, 90 °C, pH 4.5, 0.5 bar CO₂, 50 ppm Inhibitor A.

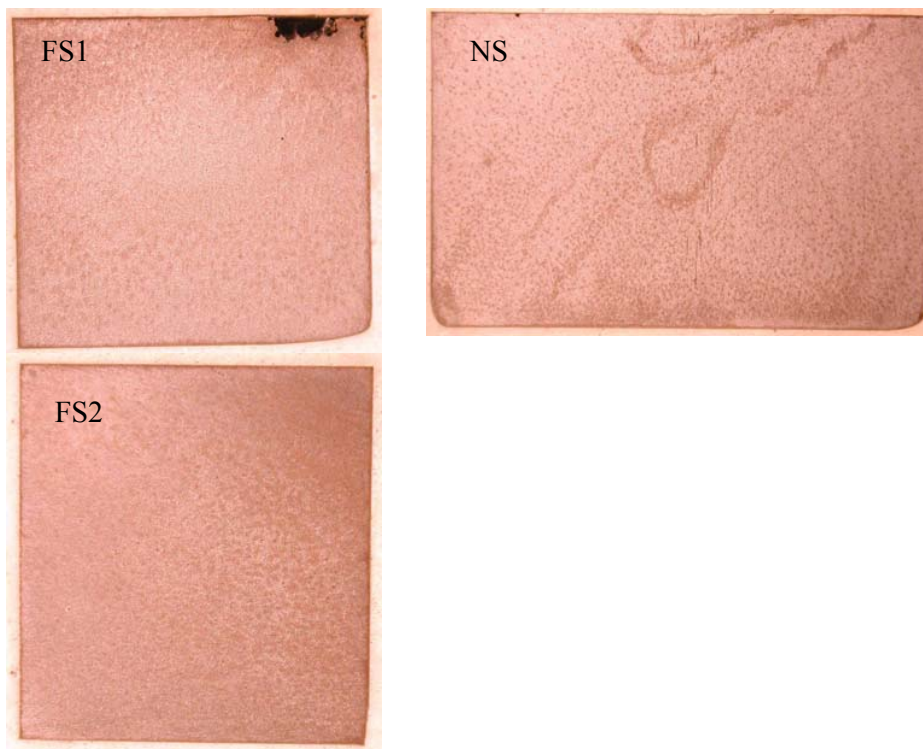


a)

Figure 12 a Caption overleaf



b)



c)

Figure 12 Results of the test when Inhibitor J was added before sand. a) LPR corrosion rates. b) Galvanic current density of the specimens.. c) Photos of the specimens after exposure. Test conditions, 10 % NaCl, 90 °C, pH 4.5, 0.5 bar CO₂, 50 ppm Inhibitor J.



Figure 13 Sand aggregation with cake formation and sand sticking to walls for a test with Inhibitor M and Oil 3. Test conditions: 10 %(w/w) NaCl, 60 °C, 0.8 bar CO₂, pH 4.5, 1 % Oil 3.



Figure 14 Sand aggregation with buoyant aggregates for a test with Inhibitor N and Oil 3. Test conditions: 10 %(w/w) NaCl, 60 °C, 0.8 bar CO₂, pH 4.5, 10 % Oil 3.

Appendix A: Polarization resistance measurements on galvanically coupled specimens

A schematic polarization curve for one of the specimens of a set of galvanically coupled specimens is shown in Figure A.1. Tafel behaviour of the partial currents is assumed for simplicity. The galvanic coupling to another specimen have polarized the specimen to the corrosion potential of the couple, E_{cor} . A galvanic current I_g' is flowing to the specimen. This is the external current, which is measured by the ZRA. This external current is the balance between the anodic (I_a') and cathodic (I_c') partial currents for this specimen. Thus at E_{cor} :

$$I_g' = I_a' + I_c' \quad (A.1)$$

The primes are used to denote the currents at E_{cor} , i.e. at the open-circuit potential of the couple.

An LPR scan is carried out by applying a small change in potential of the galvanic couple around E_{cor} . The external current I_g is measured as function of E . The polarization resistance is calculated as the gradient dE/dI_g . We want to calculate the anodic dissolution current from the measured R_p and I_g . Note that for cathodically polarized specimens the measured R_p is strongly influenced by the cathodic current, and we thus need a correction to give the anodic dissolution current. The partial currents are expressed by Tafel's law around E_{cor} . For small arguments the exponentials can be linearized ($\exp(x) \cong 1+x$), thus:

$$I_a = I_a' \exp(2.3\Delta E/b_a) \cong I_a'(1 + 2.3\Delta E/b_a) \quad (A.2)$$

$$I_c = I_c' \exp(-2.3\Delta E/b_c) \cong I_c'(1 - 2.3\Delta E/b_c) \quad (A.3)$$

Here b_a and b_c are the Tafel slopes of the anodic and cathodic curves, respectively, and $\Delta E = E - E_{cor}$. Note that the cathodic Tafel slope here is defined as an absolute value (positive). The sum of the currents are:

$$I_g = I_a + I_c = I_a'(1 + 2.3\Delta E/b_a) + I_c'(1 - 2.3\Delta E/b_c) \quad (A.4)$$

Differentiation yields:

$$dI_g = 2.3 (I_a'/b_a - I_c'/b_c) dE \quad (A.5)$$

Rearrangement gives:

$$R_p = dE/dI_g = (b_a b_c) / [2.3(I_a' b_c - I_c' b_a)] \quad (A.6)$$

Using Eq. (A.1) to substitute I_c' in Eq. (A.6) we obtain:

$$R_p = (b_a b_c) / [2.3(I_a' b_c - I_g' b_a + I_a' b_a)] \quad (A.7)$$

After some rearrangement we obtain for the anodic dissolution (corrosion) current:

$$I_a' = \frac{b_a b_c}{2.3(b_a + b_c)} \frac{1}{R_p} + I_s' \frac{b_a}{b_a + b_c} \quad (\text{A.8})$$

The first term on the right hand side is the well-known Stern-Geary expression for calculation of the corrosion current from polarization resistance at open-circuit conditions. The second term is a correction needed to obtain the true anodic dissolution rate, due to the fact that we are not measuring R_p at open circuit conditions of the single specimen, but in a polarized condition. This correction is the measured galvanic current times the factor $b_a/(b_a+b_c)$. That is, only the fraction $b_a/(b_a+b_c)$ of the galvanic current shall be added or subtracted. If $b_c = \infty$, which is commonly the case for uninhibited CO₂ corrosion (reaction limitation), the second term in Eq. (A.8) becomes zero, and the equation can be simplified to:

$$I_a' = \frac{b_a}{2.3} \frac{1}{R_p} \quad (\text{A.9})$$

Eq. (A.9) is also a good approximation if $b_c \gg b_a$, without being strictly infinite. Thus for uninhibited CO₂ corrosion, where b_a typically is found to be around 40 mV/decade, the use of a B-value of ca. 20 mV should be acceptable ($B=b_a/2.3$).

Typical data obtained for several inhibitors indicated $b_a = 50-80$ mV/decade and $b_c = 120$ mV/decade for inhibited corrosion. Thus the B-value ($B=b_a b_c / (2.3(b_a + b_c))$) becomes 15-21 mV. The use of a constant value of $B=20$ mV thus appears justified both for inhibited and uninhibited corrosion. For the inhibited case the fraction of the galvanic current used in the correction term of Eq. (A.8) became 0.3-0.4. It can be shown that in most cases the correction is small, and will not change the conclusions of the work.

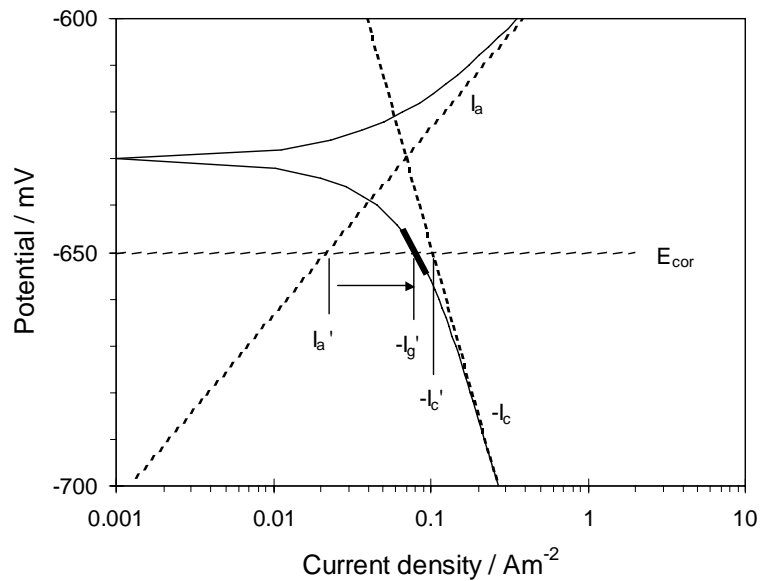


Figure A.1 Schematic polarization curve for a specimen that is cathodically polarized by the surrounding specimens. E_{cor} is the corrosion potential of the couple, I_a is the anodic dissolution current, I_c the cathodic current and I_g is the galvanic current (external current) flowing to the specimen. The short and thick straight line represents the LPR sweep around the coupled corrosion potential.